Macromolecules
ARTICLE

Macromolecules **2010**, *43*, 233–241 **233**
DOI: 10.1021/ma902009q

High Surface Area Poly(3-hexylthiophenes) Thin Films from Cleavable Graft Copolymers

Kulandaivelu Sivanandan,[†,‡,#] Tirtha Chatterjee,[†,‡,#] Neil Treat,[†,‡,§] Edward J. Kramer,*[,†,‡,§] and Craig J. Hawker*[,†,‡,§,⊥]

[†]*Mitsubishi Chemical Center for Advanced Materials,* [‡]*Materials Research Laboratory,* [§]*Materials Department,* [⊥]*Department of Chemistry and Biochemistry, and University of California, Santa Barbara, California 93106-9510.* [#] *These authors contributed equally.*

Received September 8, 2009; Revised Manuscript Received October 27, 2009

ABSTRACT: A strategy for the fabrication of high surface area poly(3-hexylthiophene) thin films by removal of nanoscale domains formed from graft copolymers is presented. This approach relies on the synthesis and characterization of cleavable graft copolymers based on regioregular poly(3-hexylthiophene) (rr-P3HT) main chain and sacrificial poly(styrene) side chains. An alkoxyamine initiator based on 2,2,6,6-tetramethylpiperidine-*N*-oxyl (TEMPO) was incorporated at the 3-position of the functionalized thienyl repeat unit, **2**, via a cleavable trityl ether linker. Grignard metathesis (GRIM) copolymerization of **2** and 2,5-dibromo-3-hexylthiophene afforded regioregular P3HT with randomly incorporated alkoxyamine groups. Polymerization of styrene from the P3HT backbone for different time periods afforded graft copolymers with controllable sacrificial chain lengths. These materials were characterized using an array of techniques such as ^{1}H and ^{13}C NMR spectroscopy and size exclusion chromatography (SEC). An approach to obtain nanoporous P3HT thin films by cleavage of the trityl ether linker followed by complete removal of poly(styrene) is reported with the as-cast graft copolymer thin films displaying an irregular microphase-separated structure with an average domain size ~30 nm as determined by grazing incidence small-angle X-ray scattering (GISAXS) measurements. Significantly, this length scale was conserved after removal of the sacrificial component which allows this strategy to have potential application in diverse fields such as organic photovoltaics.

Introduction

The possibility of inexpensive solution processing of organic photovoltaics (OPV) on flexible substrates has generated interest in these materials as alternatives to conventional inorganic semiconductor photovoltaics.[1] The development of π-conjugated polymers,[2] especially regioregular poly(3-hexylthiophenes) (rr-P3HT), and their use as p-type semiconducting (electron donor) materials have garnered significant attention due to their interesting opto/electronic properties.[3] One of the main challenges in the field of OPV is to control the thin film morphology of the active layer with this morphology playing a crucial role in device performance.[4] In OPV devices, four steps are critical for high efficiency: (i) photoexcitation of the donor and acceptors resulting in generation of excitons (hole/electron pairs), (ii) diffusion of excitons to the donor/acceptor interface, (iii) charge dissociation, and finally (iv) charge transport to the corresponding electrodes. Because of the short lifetime of the excitons, coupled with their limited diffusion length (~10−20 nm),[5] harvesting the maximum number of these excitons relies on nanoscale phase separated donor and acceptor domains with a high interfacial area.[6]

Bulk heterojunction (BHJ) architectures[7] are widely used as the active layer of organic solar cells and are fabricated by mixing rr-P3HT (electron donor) with [6,6]-phenyl-C_{61}butyric acid methyl ester (PCBM) (electron acceptor) using a common solvent and subsequently spin-casting into thin films. The phase separation between these two components creates a large interface which allows for efficient exciton formation and diffusion. In order to improve the BHJ morphology, alternate processing conditions have been investigated, such as use of different solvents to influence the solubility of P3HT and fullerene,[8] addition of small amount of processing additives (with selective solubility in one of the components) to the blend solution,[9] and thermal[10] as well as solvent annealing[11] of the thin film. However, it is believed that an ideal morphology would be an ordered BHJ consisting of alternating donor/acceptor domains, oriented perpendicular to the electrodes.[12] Such morphologies would ensure a high interfacial area with potential improvement in charge transport by providing interdigitated domains where one set of domains is connected to the anode and the other set to the cathode.

The domain size required for these systems is approximately the same size as that obtained for block copolymers which are known to self-assemble to create ordered nanostructures based on their chemical compositions and have been used as a template for the ordering of a variety of materials.[13] Nanostructured BHJ have been obtained by covalent incorporation of electron donor and acceptor groups in different segments of a self-assembling block copolymer, and successful attempts to prepare such materials have been carried out by using different conjugated polymers[14] (as donor and acceptor) as well as by incorporating a fullerene functionalized segment as the acceptor.[15] However, the difference in chain flexibilities between rod and coil segments and liquid crystalline interactions between stiff rods influence their self-assembly and subsequent nanoscale morphology.[16] Therefore, the microphase-separated microstructures of rod−coil block copolymers are different than those of their coil−coil

*Author for correspondence. E-mail: edkramer@mrl.ucsb.edu (E.J.K.) or hawker@mrl.ucsb.edu (C.J.H.).

Published on Web 11/11/2009

counterparts. Recently, Segalman and co-workers reported that weakly segregated block copolymers of poly(phenylenevinylene) (PPV) rods and poly(isoprene) (PI) coils form lamellar structures over a large range of block volume fractions below their order−disorder temperature (ODT) and not the desired cylindrical nanostructures.[17] In addition, the presence of an insulating coil segment, such as PI, in the solar cell active layer, however, would dilute any fullerene component and probably decrease the mobility of the charge carriers.[18,19]

An alternative approach to obtaining high interfacial area between the donor and acceptor domains is to create a highly porous rr-P3HT film followed by backfilling with an acceptor material. While a variety of strategies are possible for the formation of highly porous rr-P3HT films, degradation of rr-P3HT copolymers was considered to be the most viable strategy based on domain size and ease of fabrication. In this case etching of the sacrificial domain can be achieved using two methods: (i) either by choosing a sacrificial polymer that can be degraded to small molecular fragments[20] or (ii) by incorporation of an orthogonal cleavable linker and selective removal of the sacrificial polymer.[21] For efficiency, it was decided to synthesize a series of P3HT-based copolymers containing a cleavable linker, and to overcome the challenge of P3HT block copolymer synthesis,[22] we report a simple strategy to obtain porous rr-P3HT films from cleavable graft copolymers containing a rr-P3HT main chain and sacrificial poly(styrene) (PS) side chains. The starting P3HT macroinitiator was obtained by copolymerization of a TEMPO-containing thienyl repeat unit **2** with 2,5-dibromo-3-hexylthiophene. Polystyrene was then grafted from the rr-P3HT backbone using living free radical polymerization techniques, and in contrast to the traditional postsynthetic modification of P3HT,[23] this "growth-from" strategy provides for precise control over the grafting density by controlling the feed ratio as well as the ability to graft different sacrificial vinyl-based polymers such as poly(vinylpyridine) and poly(hydroxystyrene), etc. These features allow copolymers with different chemical compatibility and composition to exhibit modified self-assembly behavior which provides for a range of nanostructures.

Experimental Section

^{1}H NMR spectra were recorded on a Bruker DMX-500 MHz NMR spectrometer using the residual proton resonance of the solvent as internal standard. ^{13}C NMR spectra were proton decoupled and recorded at 125 MHz using the carbon signal of the deuterated solvent as the internal standard. Chemical shifts are reported in parts per million (δ) relative to $CHCl_3$ (7.27 ppm for ^{1}H and 77.0 ppm for ^{13}C) as internal reference. When peak multiplicities are given, the following abbreviations are used: s, singlet; d, doublet; t, triplet; q, quartet; qt, quintet; m, multiplet; bs, broad singlet. Size exclusion chromatography (SEC) was performed in tetrahydrofuran (THF) on a Waters 2695 separation module equipped with a Waters 2414 refractive index detector and a Waters 2996 photodiode array detector. UV−vis absorbance spectra were obtained on a Shimadzu UV-3600 spectrometer with a 60 mm integrating sphere.

Materials. Commercial reagents were obtained from Aldrich and used without further purification unless otherwise noted. THF was distilled over Na/Ph_2CO ketyl and styrene was passed through basic alumina before being used for polymerizations. Deuterated solvents and d_8-styrene were obtained from Cambridge Isotope Laboratories, Inc. Flash chromatography was performed with EM science 37−75 μm silica gel. Analytical thin layer chromatography was performed on EM science silica plates with F-254 indicator, and visualization was accomplished by UV lamp or molybdic acid as a stain.

Thin Film Preparation, Cleavage of Trityl Ether Linker, and Selective Removal of Poly(styrene). A 1 wt % solution of P3HT-*g*-PS in toluene was spin-coated on a silica substrate at a speed of 3000 rpm and dried under ambient conditions for 20 min. The average film thickness, measured using X-ray reflectometry, was found to be 35 ± 5 nm. Later the thin film was mounted on top of a vial, which was already placed in a larger vial containing TFA. The larger vial was sealed with a screw cap. After 2 h, the thin film was taken out of chamber, soaked into stirring DMF (100 mL) for 30 s to selectively remove PS, and then dipped into methanol (to remove any residual DMF). The thin film was dried under ambient conditions for 10 min and used for characterizations.

Scanning Force Microscopy (SFM). Tapping mode SFM was performed using either a Veeco Metrology Group Digital Instrument Dimension 3000 or 3100 instrument. Commercially available Si cantilevers (nominal spring constant and resonance frequency in the range of 20−95 N/m and 145−230 kHz, respectively) were used for all the measurements. The height and phase images were acquired simultaneously while controlling the set point ratio ($S = A/A_0$, where A and A_0 are the tapping and free cantilever amplitudes, respectively). The typical S values used in this study range from 0.8 to 1.0. The typical scan size was 2.0 μm × 2.0 μm, and data were stored at a resolution of 512 × 512 pixels per image.

Grazing Incidence Small-Angle X-ray Scattering (GISAXS). These experiments were conducted on the sector 8-ID-E beamline at Advanced Photon Source (APS), Argonne National Laboratory (ANL). The wavelength of the incident X-ray beam was 1.687 Å, and the sample-to-detector distance was 1991.0 mm as determined from calibration with a silver behenate standard (d = 58.376 Å). For each sample, typically four incident angle measurements were carried out with one angle just below the polymer critical angle ($\alpha_{poly,cr}$), and one angle just above the substrate critical angle ($\alpha_{sub,cr}$). The other two measurements were performed in between these two critical angles ($\alpha_{poly,cr} < \alpha_i < \alpha_{sub,cr}$), and the selection was based on the appearance of minima in X-ray reflectivity data (correspond to X-ray standing waves in the film with different periods). The off-specular scattering data were recorded as a function of in-plane and out-of-plane diffraction angles with a 2D MAR-CCD detector with pixel size 0.079 mm. Finally, each data set was stored as a 2048 × 2048 16-bit TIFF image.

Dynamic Secondary Ion Mass Spectrometry (d-SIMS). The depth profiling experiment was carried out on a Physical Electronics 6650 quadrupole system (Chanhassen, MN) SIMS instrument using a 40 nA, 2 keV primary ion beam of O_2^+ ions at an incidence angle of 60° to the surface normal. A spot size of 30 μm was rastered over a 300 μm wide crater area. The secondary ion signal was collected from the central 15% of the crater area. Charging of the sample was avoided by neutralizing the sample with a static defocused electron beam (0.2 keV). The negative ions of H, D (specific to dPS), C, S (specific to rr-P3HT), and Si were monitored as a function of time and subsequently correlated with the sample thickness using the sputtering rate. The typical interface depth resolution of this technique is ~5−10 nm.

Alkoxyamine−Thiophene Initiator 2. A solution of the trityl chloride **1** (1.53 g, 2.7 mmol) in freshly distilled THF (10 mL) was added dropwise to a stirring solution of 2,5-dibromo-3-(11-hydroxyundeceyl)thiophene[24] (1.33 g, 3.24 mmol), pyridine (0.65 mL, 8.1 mmol), and Ag(OTf) (0.7 g, 2.7 mmol) in freshly distilled THF (20 mL). The reaction mixture was stirred at room temperature for 4 h under an argon atmosphere, and after completion of the reaction, THF was removed by rotary evaporation and the crude product was dissolved in CH_2Cl_2 and subjected to water work-up. The aqueous layer was extracted twice with CH_2Cl_2, and the combined organic layer was passed over anhydrous magnesium sulfate. Evaporation of CH_2Cl_2 afforded the crude product which was purified by silica gel column chromatography using ethyl acetate/hexane (5:95) solvent mixture to give **2** as a colorless solid. Yield 1.8 g (60%). ^{1}H NMR (500 MHz, $CDCl_3$): δ 7.50−7.15 (m, 16H),

Scheme 1. Synthesis of P3HT-*g*-PS Copolymers, 4a−c, from the Functionalized Thiophene, 2

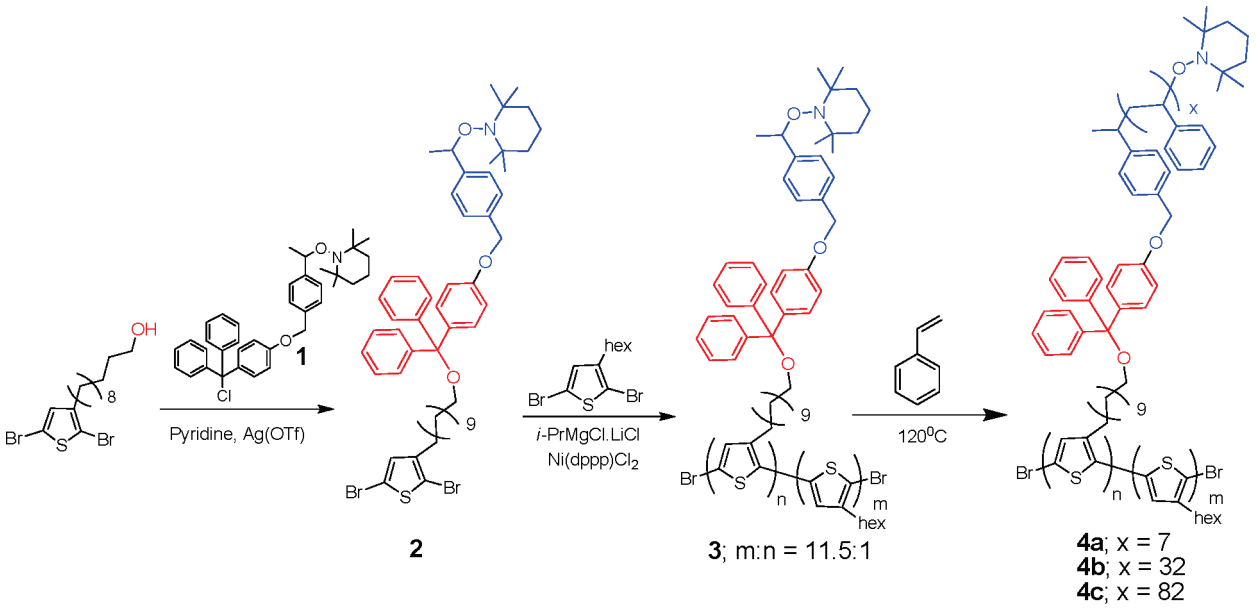

6.91 (d, J = 8.9 Hz, 2H), 6.78 (s, 1H), 5.02 (s, 2H), 4.80 (q, J = 6.6 Hz, 1H), 3.05 (t, J = 6.6 Hz, 2H), 2.50 (t, J = 7.6 Hz, 2H), 1.70−0.60 (m, 39H). ^{13}C NMR (125 MHz, $CDCl_3$): δ 157.6, 145.5, 144.9, 142.8, 136.4, 135.3, 130.8, 128.3, 127.7, 127.2, 126.7, 126.5, 113.7, 107.8, 85.8, 82.7, 69.9, 63.5, 59.6, 40.3, 34.4, 34.1, 30.0, 29.4, 29.4, 29.4, 29.2, 29.0, 26.2, 23.4, 20.3, 17.1. FABMS (NBA) m/z: 944 (M^+).

Macroinitiator 3. 2,5-Dibromo-3-hexylthiophene[25] (1.44 g, 4.43 mmol), **2** (0.27 g, 0.3 mmol), and Ni(dppp)Cl_2 (51 mg, 0.09 mmol) were placed in a three-necked round-bottom flask and dissolved in freshly distilled THF (55 mL). The solution was cooled to 0 °C, and freshly prepared *i*-PrMgCl·LiCl[26] in THF (4.7 mL, 1 M solution) was added dropwise. The reaction was allowed to stir for 1 h at 0 °C under an argon atmosphere with the reaction mixture turning dark red in color. After this time, the reaction mixture was concentrated and added to 500 mL of methanol to precipitate the polymer. The polymer was filtered and transferred to an extraction thimble and washed extensively with methanol and hexanes using a Soxhlet apparatus. The purified polymer was then extracted using chloroform. Yield 0.5 g (75%). ^{1}H NMR (500 MHz, $CDCl_3$): δ 7.60−7.10 (m, 18H), 6.99 (s, 15H), 5.01 (s, 2H), 4.78 (m, 1H), 3.04 (t, J = 7.5 Hz, 2H), 2.90−2.50 (m, 30H), 1.90−0.60 (m, 201H); GPC: M_n = 13 000 g mol^{-1}, PDI = 1.15.

Results and Discussion

The synthesis of the desired P3HT-*g*-PS copolymers, **4a−c**, is depicted in Scheme 1 with the first step involving alkylation of 2,5-dibromo-3-(11-hydroxyundecane)thiophene[24] with the alkoxyamine,[25] substituted trityl chloride **1** (see Supporting Information for synthesis of **1**) using pyridine as the base and Ag(OTf) as the catalyst. This afforded the modified thienyl repeat unit **2** in 60% yield. Grignard metathesis (GRIM) copolymerization of **2** and 2,5-dibromo-3-hexylthiophene[26,27] then gave the rr-P3HT macroinitiator, **3**, with randomly incorporated alkoxyamine initiating groups. The copolymer, **3**, could be purified by precipitation in methanol followed by sequential Soxhlet extraction using methanol and hexane. Significantly, the use of an inimer strategy provides the ability to vary the structure of the copolymer by controlling the feed ratio of **2** and 2,5-dibromo-3-hexylthiophene. For example, if $m \gg n$ (Figure 1, low grafting density), a copolymer with a blocklike structure is obtained, while for $m \ll n$ (higher grafting density), a much different comblike structure is obtained. This variation in the number of initiating groups along the backbone leads to copolymers with different grafting densities and distinct phase separation behavior that can be utilized to control the thin film morphology of P3HT.

To demonstrate morphology control, styrene was grafted from the macroinitiator **3** using nitroxide-mediated polymerization (NMP) techniques with the reactions being performed in sealed ampules under an oxygen-free atmosphere at 120 °C. Graft copolymers with different PS weight percentage (**4a−4c**) were synthesized by controlling the polymerization time (Table 1) and subsequently purified by precipitation in methanol. Of particular note was the observation that the alkoxyamine group is stable to the GRIM polymerization conditions used for growth of the poly(thiophene) backbone. In contrast, ATRP initiators contain an active halogen atom or carbonyl group, which can undergo a metal−halogen exchange or a possible Grignard addition. Grafting from poly(thiophenes) (PT) using ATRP has been reported and was achieved either by postsynthetic modification of rr-PT or by oxidative polymerization of ATRP-functionalized thiophene.[28] The postsynthetic modification is not efficient and time-consuming, whereas the second approach of oxidative polymerization does not yield rr-PT and control of the molecular weight is difficult.

Full characterization of the macroinitiator, **3**, was achieved using a variety of spectroscopic and chromatographic techniques which revealed a close correlation between the feed ratio of **2** and its actual incorporation. The stability of **2** under the GRIM conditions can be evidenced in Figure 1, which shows the ^{1}H NMR spectrum of macroinitiator **3** and the presence of a quartet at 4.8 ppm (c), singlet at 5.0 ppm (b), and triplet at 3.0 ppm (d), all due to the functionalized alkoxyamine side chain. The level of alkoxyamine incorporation in polymer **3** was determined by integrating the area of methylene protons of the trityl ether (d, 3.0 ppm) against the main chain protons of poly(thiophenes) at 7.0 ppm (a, Figure 1). For the copolymers studied, the average m to n ratio was estimated to be 11.5:1, which is close to the feed ratio (14:1).

Similarly, growth of the polystyrene grafts was apparent through NMR spectroscopy and size exclusion chromatography (SEC) with the ^{1}H NMR spectrum of a representative graft copolymer **4a** shown in Figure 2. The degree of polymerization of styrene (x) was determined by comparing the integration values

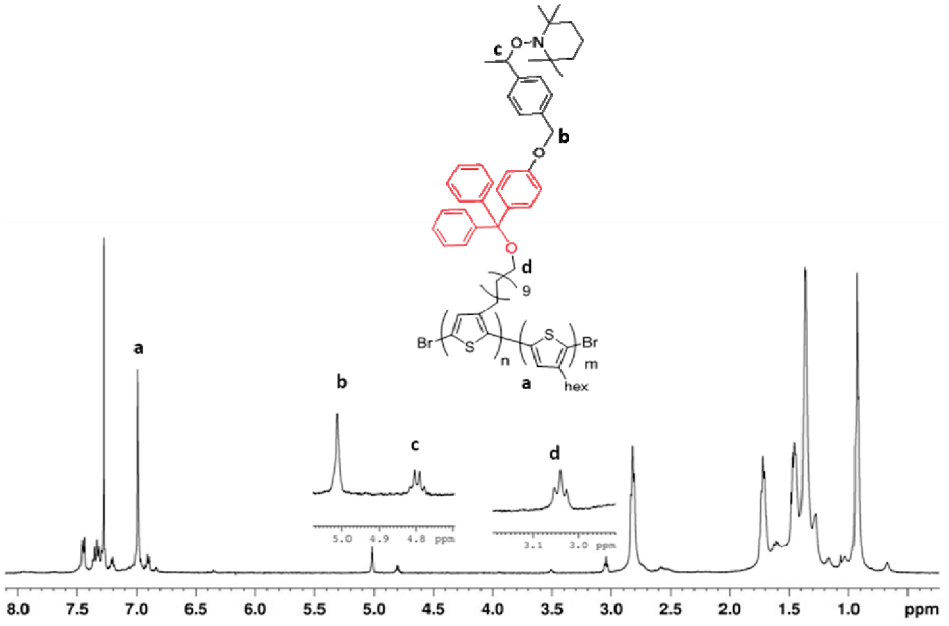

Figure 1. ^{1}H NMR spectrum of P3HT-based macroinitiator **3** in $CDCl_3$. The peaks upfield of 2.0 ppm are associated with the alkyl side chains and the TEMPO groups. The unlabeled peaks downfield of 6.7 ppm represent the aromatic protons of the trityl and TEMPO groups with the minor peak at ca. 3.50 ppm being due to trace amounts of residual methanol from precipitation.

Table 1. Characterization of Macroinitiator 3 and the Graft Copolymers 4a−4b

sample	polymerization time (min)	conversion (%)	n:m:x[a]	PS[a] (wt %)	M_n[b] (g/mol)	M_w/M_n[b]
3			1:11.5:0		13 000	1.1
4a	30	52	1:11.5:7	36	50 000	1.5
4b	60	64	1:11.5:32	64	74 000	1.5
4c	90	70	1:11.5:82	80	90 000	1.6

[a] Determined by ^{1}H NMR spectroscopy. [b] Determined by SEC.

of the poly(styrene) aromatic protons (a) and the side chain, hexyl resonances of compound **3** (d). The value of x and the poly(styrene) weight percentage in graft copolymers **4a−4c** were also calculated and reported in Table 1. The molecular weights of macroinitiator **3** and graft copolymers **4a−4c** were determined by size exclusion chromatography (SEC). Because of the rodlike structure of poly(thiophenes), the molecular weight obtained by SEC using poly(styrene) standards can be higher than the actual molecular weight.[29] The weight percentage of poly(styrene) in compounds **4a−4c** was also determined by ^{1}H NMR spectroscopy and correlated with the expected values from conversion and feed ratios.

Size exclusion chromatography (SEC) of compound **3** (Figure 3) with both refractive index and UV−vis detection indicated a narrow molecular weight distribution (M_w/M_n = 1.15), which is typical for the GRIM polymerization with a high molecular weight shoulder being observed due to chain−chain coupling. From the well-defined poly(thiophene) backbone, relatively monomodal distribution for the graft copolymers indicates almost complete initiation of grafted chains from **3** with a shoulder for unreacted P3HT only being significant for **4a**. The presence of a shoulder for **4a** is due to the low incorporation of **2**, leading to a statistically significant population of chains with no alkoxyamine units present along the backbone. Additionally, the difference in the retention time between macroinitiator **3** and graft copolymer **4a−4c** is attributed to the change in the hydrodynamic volume upon increase in molecular weight. However, within graft copolymers (**4a−4c**), only a slight decrease in the elution time with increase in poly(styrene) chain length was observed.

To demonstrate the degradation of the trityl ether linker in the solid phase, **4c** was drop-cast on a glass slide and the resulting thin film was exposed to CF_3COOH (TFA) vapor for a period of 2 h. Size exclusion chromatography (SEC) with both refractive index and UV−vis detection was then performed on the dissolved products and compared with the original graft copolymer (**4c**). As shown in Figure 4, complete disappearance of the peak for **4c** and the appearance of a new signal at higher retention time, corresponding to a mixture of P3HT and PS homopolymers resulting from cleavage of the trityl ether linkers, were observed. In the case of **4c**, they appear as a single peak; however, analysis of the signal by photodiode array detector indicated a strong absorption between 400 and 500 nm, confirming the presence of P3HT homopolymer (Figure S2, Supporting Information).

To gain a preliminary understanding of the effect of TFA vapor exposure and associated cleavage of the trityl group on the poly(thiophene) backbone, the optical and electrical properties of the poly(thiophene) was examined. For high performance, these properties should not be affected during the degradation process. UV−vis absorption spectroscopy of the graft copolymer films under various conditions was therefore studied with initial broadening of the P3HT absorption at higher wavelength, indicating oxidation of the conjugated polymer by TFA (Figure 5).[30] This is in agreement with literature reports which detail the intentional p-type doping of P3HT with TFA to increase conductivity and environmental stability.[31] In this process, oxidation of the conjugated polymer occurs by losing two electrons to form a bipolaron[32] that has a broad absorption from 500 to 1100 nm. A similar behavior was observed after treating the graft copolymers with TFA; however, upon rinsing these films with triethylamine the optical property of P3HT was almost fully restored.

Thin Film Characterization. Having confirmed the structure and degradation behavior of the graft copolymers, the morphology and surface properties of the as-cast thin films were then investigated using tapping mode scanning force microscopy (SFM). The topography and phase images of a representative graft copolymer film (**4c**) are shown in Figure 6a with the topography image showing a smooth surface and the surface roughness decreasing with increasing PS content.

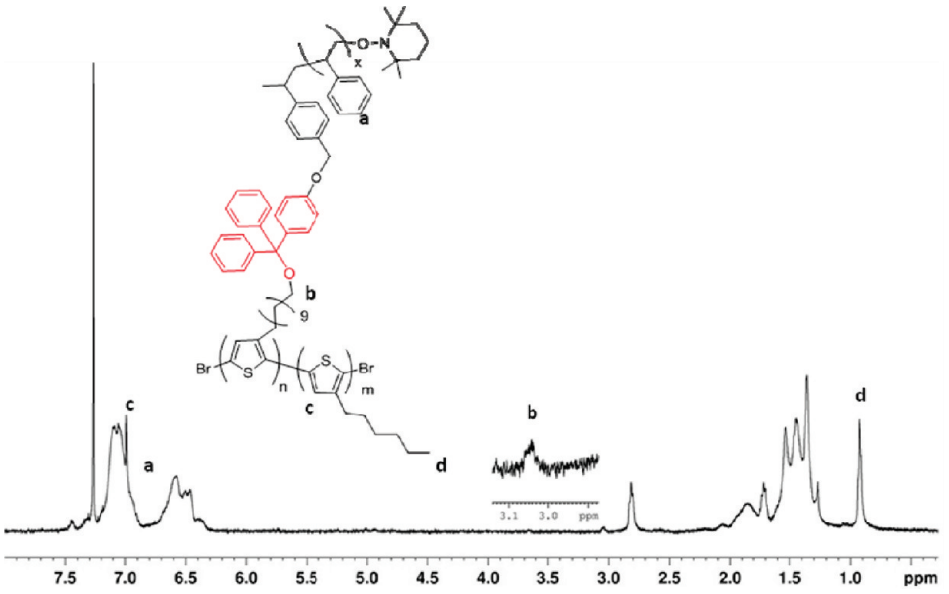

Figure 2. ^{1}H NMR spectrum of P3HT-*g*-PS **4a** in $CDCl_3$. The peaks upfield of 2.0 ppm are associated with alkyl side chains and poly(styrene) backbone.

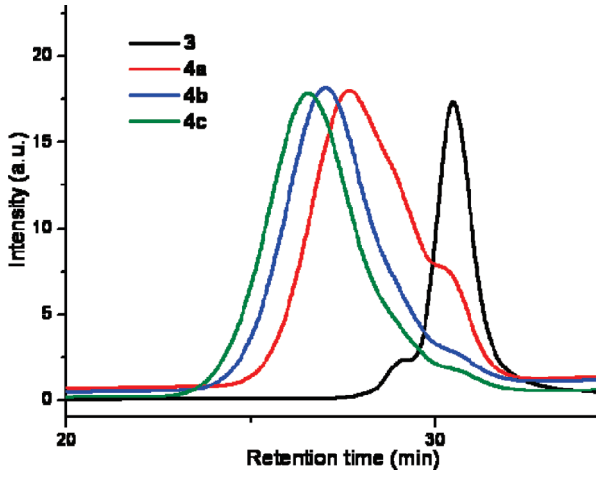

Figure 3. SEC traces of the macroinitiator **3** and the graft copolymers **4a**−**4c** with different poly(styrene) content.

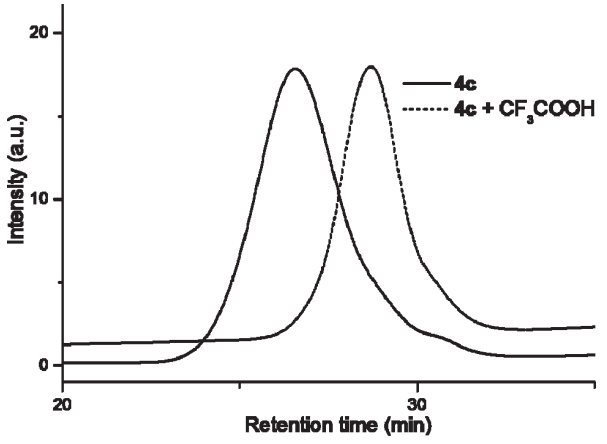

Figure 4. SEC trace of the graft copolymer **4c** before and after TFA treatment.

For example, the root-mean-square (rms) roughness decreases from 1.2 ± 0.1 to 0.2 ± 0.0$_4$ nm when the PS wt % increases from 36 (**4a**) to 64 (**4b**), respectively. In order to obtain information on the P3HT nanostructures, hard tapping ($S \sim 0.8$) was employed as previously reported by McCullough and co-workers.[19] The phase image indicates a phase-separated structure with the presence of disordered P3HT nanocrystallites. After etching of the polystyrene, a significant increase in the film roughness was observed (Figure 6b) with this increase arising from porosity formed during removal of the PS domains. A control sample, where the thin film (**4c**) was washed only with DMF (no TFA vapor exposure), did not show any significant roughness (Figure S3, Supporting Information).

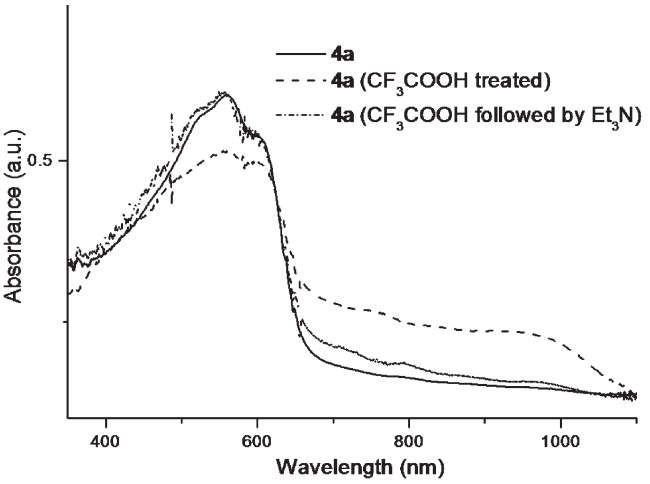

Figure 5. UV−vis absorption spectroscopy of the graft copolymer thin films before and after TFA vapor exposure. Neutralization of the thin films with triethylamine (Et_3N) restores poly(thiophenes) absorption.

In all P3HT-*g*-PS samples, while the grafting density is similar, the degree of polymerization of styrene is varied (Table 1). This leads to similar backbone structures with the higher PS content giving rise to longer PS chains, and it is expected that upon removal of the sacrificial component the samples with higher PS content will demonstrate a greater degree of film roughness/porosity. This increase in film roughness is clearly evident from the 3-dimensional (3D) topographic view of the SFM profiles (Figure 7). For the

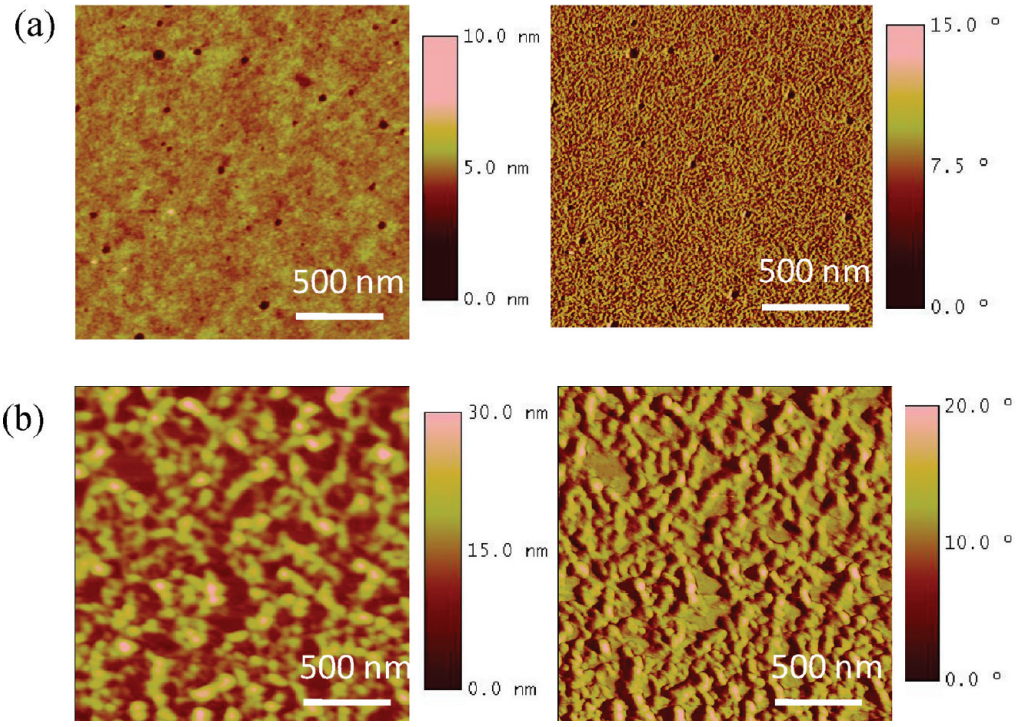

Figure 6. (a) Tapping mode SFM topography (left) and phase (right) images of the as-cast **4c** copolymer thin film on Si/SiO_x substrate. The topography image shows a smooth film surface, whereas P3HT nanocrystallites are clearly visible in the phase image. (b) Topography and phase image of the same film after removal of the PS. The surface roughness increases due to nanopore formation, and a considerable change in the phase image is also observed.

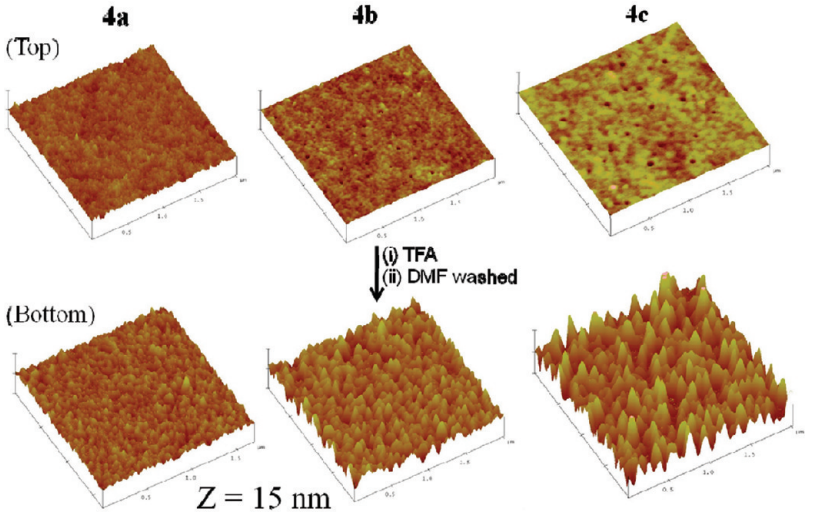

Figure 7. 3D topography view of different P3HT-*g*-PS thin films before and after PS removal. In all the cases the images were built from 2 μm × 2 μm SFM height scans. Clearly, removal of PS from the thin film resulted in increase in roughness. The total height range is 15 nm for all the images.

as-cast graft copolymers (top row, Figure 7), 3D topographic views show little change in the surface across the scan area. However, after removal of the PS (bottom row, Figure 7), formation of porosity in the thin film surface is observed with the rms roughness values being 2.2 ± 0.1, 3.7 ± 0.4, and 3.8 ± 0.3 nm for samples **4a**, **4b**, and, **4c**, respectively. While these images suggest a higher pore penetration depth for high PS content samples, accurate depth measurement is limited by the tip resolution. Nevertheless, the scanning force microscope image do demonstrate trend in increasing surface roughness with removal of increasing PS content.

Grazing incidence small-angle X-ray scattering (GISAXS) experiments were then performed to understand the morphology of the thin films before and after etching. For a two-domain system, the X-ray scattering intensity is directly proportional to the square of the difference in their electron densities with for the as-cast sample scattering intensity being proportional to $(\rho_{P3HT} - \rho_{PS})^2$. However, after PS removal, the scattering intensity should be proportional to $(\rho_{P3HT} - \rho_{vac})^2$, where the ρ's are the electron densities of P3HT, PS, and vacuum ($=0$). Therefore, when the PS is removed, an increase in intensities is expected. A representative in-plane scattering intensity of the graft copolymer thin film (**4a**) before and after PS removal is presented in Figure 8. For direct comparison, the measurements were performed at the same incident angles, and the scattering intensities were

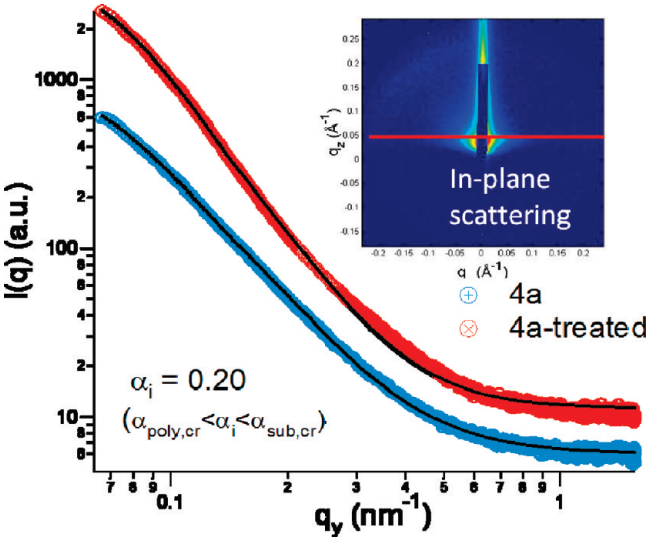

Figure 8. GISAXS in-plane line profile for a representative graft copolymer before and after PS removal. The data were collected for same exposure time and an incident angle between the polymer and substrate critical angle. Solid lines are model fit to the experimental data. (inset) 2D GISAXS intensity profile showing the fixed out-of-plane scattering vector at which in-plane line profile was obtained.

corrected for the incoming X-ray beam intensity and the exposure time. For all the intermediate incident angles ($\alpha_{poly,cr} < \alpha_i < \alpha_{sub,cr}$) investigated, the sample from which PS has been removed showed higher intensity which provides additional evidence of successful removal of PS throughout the depth of the film.

In all cases, the in-plane scattering profile (Figure 8) is featureless and resembles that characteristic of disordered domains. Similarly, the out-of-plane scattering (data not shown) is also featureless, demonstrating a lack of ordering throughout the thickness of the sample. These results indicate the lack of long-range order in these graft copolymers and is consistent with the SFM results. Moreover, the in-plane scattering profile for **4a** is almost identical before and after the etching process. This implies that for the length scale accessed through GISAXS measurements (~4.5−90 nm) the P3HT microstructure is not significantly disturbed by the PS removal process. Small changes were observed in the scattering profile (especially at low in-plane scattering vector (q_y)) before and after PS removal for the highest PS sample **4c**, which is due to the significant mass removal which disturbs the arrangement of the minor P3HT domains (Figure S4, Supporting Information).

One of the important criteria of bulk heterojunction architecture is creation of domain size comparable to the exciton diffusion length. To obtain the characteristic domain size, the scattering data were fitted using a unified equation[33] expressed as

$$I(q_y) = G\exp\left(-\frac{q_y^2 R_g^2}{3}\right) + B\left\{\left[erf\left(\frac{q_y R_g}{\sqrt{6}}\right)\right]^3/q_y\right\}^{pow} + bgd \qquad (1)$$

where the scattering from the disordered domain is represented as a combination of the Guinier scattering at low q_y and structurally limited power law scattering at higher q_y, considering both as independent scattering sources.

Table 2. Unified Model Fit Results of the Scattering Data for P3HT-*g*-PS System before and after PS Removal

sample	processing	length scale (R_g) (nm)	power law exponent (*pow*)
4a	as-cast	27.2 ± 3.6	$2.9 \pm 0.0_3$
4a	treated	28.8 ± 4.4	3.6 ± 0.3
4c	as-cast	30.2 ± 5.0	$2.5 \pm 0.0_1$
4c	treated	33.0 ± 0.6	$3.6 \pm 0.0_7$

Here G and B are Guinier and power law scattering prefactors, respectively, and *bdg* is a constant background. The average characteristic domain length and the associated fractal dimension are given by R_g and *pow*, respectively. For a mass fractal system, *pow* lies between 2.0 and 3.0, whereas for a surface fractal *pow* is between 3.0 and 4.0. Equation 1 is applied to obtain the average size of the microphase-separated domains, and the corresponding fractal dimension (*pow*) for grafted copolymer system and the extracted parameters are reported in Table 2. The first thing to notice is that the average domain size increases slightly after the PS removal process. This change in the domain size is more prominent for the high PS content sample (**4c**), where removal of long grafted PS chains disturbs the underlying P3HT organization. However, the change in domain size after PS removal is quite small (≤10% of the as-cast domain size), and hence we infer that the PS removal process does not alter the microphase-separated structure significantly. Interestingly, for all the samples, a substantial change in the fractal dimension was observed. The as-cast thin films resemble a mass fractal system, whereas after the etching process it behaves as a surface fractal. The fractal dimension between 3 and 4 characterizes the rough interface arising from pore formation.

The scanning force microscopy and X-ray measurements demonstrate selective removal of PS to obtain nanoporous P3HT film. However, it is also important to understand the effectiveness of the PS removal process, i.e., to ensure complete removal of PS from the thin film. Therefore, monitoring the amount of residual PS left after PS removal as a function of depth within the film is essential. Determining the depth distribution of an organic component in a composite thin film, where both components do not have a distinctive element, can be accomplished by labeling one of the components with deuterium (D) in combination with dynamic secondary ion mass spectrometry (d-SIMS).[34] For depth profiling, a graft copolymer with deuterated PS (dPS) sacrificial component (P3HT-*g*-dPS) was therefore synthesized (Supporting Information). As a buffer layer, a *free-standing* protonated PS film was placed on top of the samples. The thicknesses of the P3HT-*g*-dPS and protonated PS films were determined to be 39 ± 2 and 78 ± 3 nm, respectively, from X-ray reflectometry measurements.

Figure 9a shows the secondary ion intensity as a function of the film thickness for the control sample (without TFA treatment). Different secondary ion intensities were monitored as a function of time and related to the film thickness using the sputtering rate. Deuterium ion intensity allowed the location of the dPS chains to be probed while S ion (specific to the thiophene rings) intensity was tracked to determine the distribution of the P3HT chains. Initially, the sputtering occurred at the buffer PS layer as evident from the strong C and H ion intensities (Figure 9a). During this period, S, D, and Si secondary ion intensities remained negligibly small. The transition from the PS to underlying P3HT-*g*-dPS layer was confirmed by the simultaneous increase in for both S (specific to P3HT chains) and D (specific to dPS chains) ion intensities. The copolymer film thickness (39 nm) was much higher than the depth resolution of the

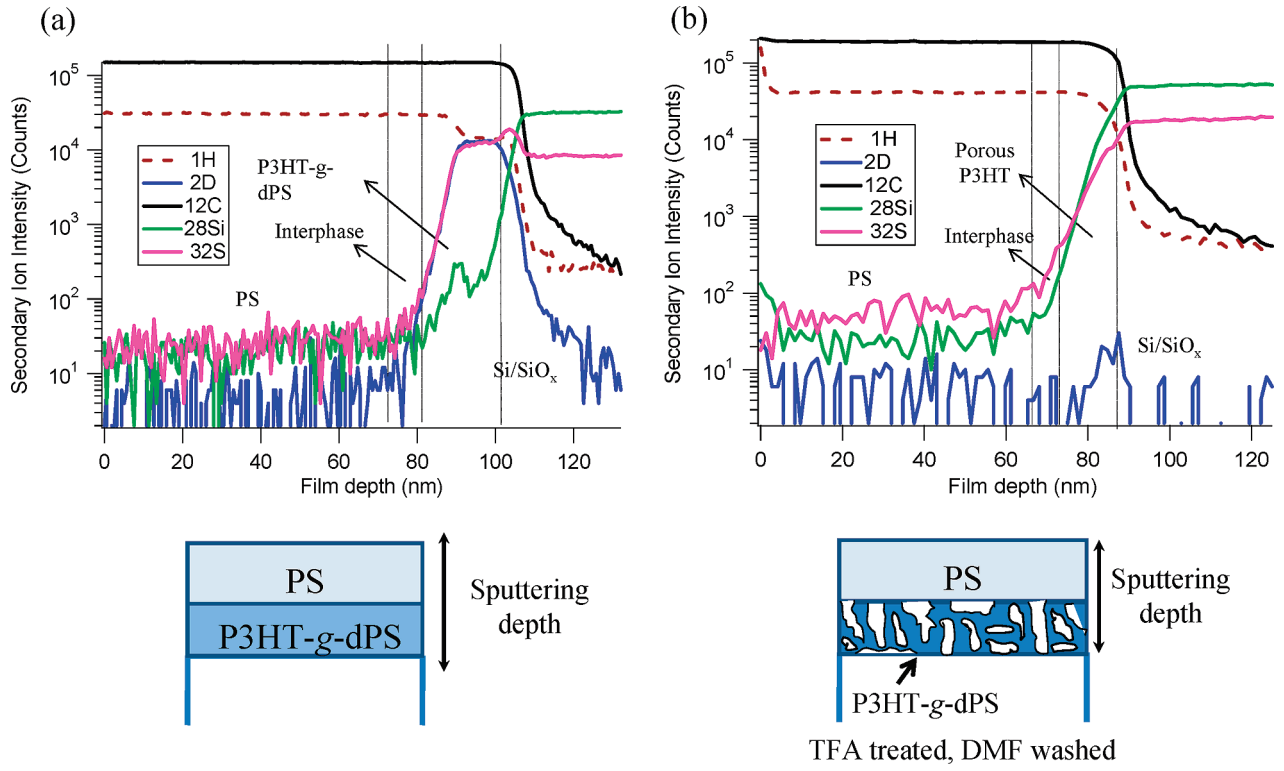

Figure 9. (a) d-SIMS depth profile for P3HT-*g*-dPS sample before etching. The presence of dPS chains throughout the sample thickness was evident from strong ^{2}D ion signal. (b) d-SIMS depth profile after dPS removal. The absence of any strong ^{2}D ion signal proved the complete removal of dPS segment and nanopore formation along the film thickness. Note in both cases a *free-standing* PS film was placed on the top of the graft copolymer film as a buffer layer.

d-SIMS instrument (~10 nm), and strong identical D and S signals suggest homogeneously distributed copolymer morphology along the film depth. As the sputtering depth reached the bottom of the graft copolymer layer, the deuterium, carbon, and hydrogen signals dropped sharply with a concomitant increase in silicon ion count. The sulfur signal still maintained the steady ion count due to sputtering of oxygen ions (O_2 molecular mass is 32, same as sulfur) from the substrate oxide layer. Nevertheless, the depth profiling showed dPS-rich domains uniformly distributed along film thickness and ruled out the possibility of any spontaneous stratification.

Figure 9b represents the secondary ion intensity as a function of the film thickness for the P3HT-*g*-dPS sample after TFA treatment and washing to remove PS chains. Initially, the ion counts were essentially the same as the control sample with the sputtering occurring in the buffer hydrogen containing PS layer. However, as the P3HT layer was reached, sputtering produced only a strong sulfur ion signal with the deuterium ion signal remaining at essentially baseline levels. This weak D signal actually arises from the presence of the natural abundance of ^{2}H isotopes (one out of 6000 hydrogen atoms) in protonated PS and P3HT molecules. This absence of D signal demonstrates that the dPS chains are completely removed throughout the film thickness and indicates that porosity penetrates the entire depth of the film.

Summary

The synthesis and characterization of cleavable graft copolymers based on a functionalized P3HT backbone are reported. The PS chains were grafted from P3HT-based macroinitiators containing randomly incorporated alkoxyamine groups using nitroxide-mediated polymerization with acid sensitive trityl ether being used to covalently link the P3HT and the PS segments. This strategy allows porous P3HT films to be prepared through selective cleavage of the PS grafts by exposure to TFA vapor followed by washing with DMF. The as-cast graft copolymer thin films exhibited a smooth surface with phase-separated disordered domains; however, upon removal of the PS grafts, the surface roughness increases due to pore formation, with the characteristic domain length of the graft copolymers (20−30 nm) being preserved even after removal of the PS component. Complete removal of PS throughout the film thickness was demonstrated by d-SIMS measurements with the extent of thin film porosity being controlled by the PS chain length. This study offers a convenient strategy for the preparation of highly porous P3HT thin films with controlled porosity which offer promise as high surface area scaffolds for a variety of applications such as sensors and organic photovoltaics.

Acknowledgment. Financial support from Mitsubishi Chemical Center for Advanced Materials (MC-CAM), Mitsubishi Chemical Group Science and Technology Research Center, Inc., NSF ConvEne IGERT Program DGE-0801627, and the central facilities of the UCSB Materials Research Laboratory (NSF Grant DMR05-20415) is gratefully acknowledged. Use of the GISAXS facility (sector 8-ID-E beamline) at APS was supported by the US DOE Office of Basic Energy Sciences, under Contract DE-AC02-06CH11357. We thank Dr. Michael Sprung, Dr. Alec Sandy, Dr. Suresh Narayan, Dr. Joseph Strzalka, and Dr. Jin Wang for help with the GISAXS measurements. Thanks to Dr. Tom Mates for help with the d-SIMS measurements. We also thank Professor Michael Chabinyc, Dr. Roey Amir, and Jasmine Hunt for helpful discussions.

Supporting Information Available: Synthesis and characterization of compound **1**, graft copolymers **4a**−**4c**, and P3HT-*g*-dPS. This material is available free of charge via the Internet at http://pubs.acs.org.

References and Notes

(1) (a) Hoppe, H.; Sariciftci, N. S. *J. Mater. Chem.* **2006**, *16*, 45–61. (b) Mayer, A. C.; Scully, S. R.; Hardin, B. E.; Rowell, M. W.; McGehee, M. D. *Mater. Today* **2007**, *10*, 28–33. (c) Nelson, J. *Curr. Opin. Solid State Mater. Sci* **2002**, *6*, 87–95.

(2) Heeger, A. J. *J. Phys. Chem. B* **2001**, *105*, 8475–8491.

(3) (a) Bolognesi, A.; Pasini, M. C. Synthetic methods for semiconducting polymers. In *Semiconducting Polymers*, 2nd ed.; Hadziioannou, G., Malliaras, G. G., Eds.; Wiley-VCH Verlag GmbH & Co. KGaA: Berlin, 2007; Vol. *1*, pp 1−68. (b) McCullough, R. D. *Adv. Mater.* **1998**, *10*, 93–116.

(4) (a) Peet, J.; Senatore, M. L.; Heeger, A. J.; Bazan, G. C. *Adv. Mater.* **2009**, *21*, 1521–1527. (b) Lee, Y.; Fukukawa, K. I.; Bang, J.; Hawker, C. J.; Kim, J. K. *J. Polym. Sci., Polym. Chem.* **2008**, *46*, 8200–8205. (c) Durben, S.; Nickel, D.; Krüger, R. A.; Sutherland, T. C.; Baumgartner, T. *J. Polym. Sci., Polym. Chem.* **2008**, *46*, 8179–8190.

(5) (a) Markov, D. E.; Hummelen, J. C.; Blom, P. W. M.; Sieval, A. B. *Phys. Rev. B* **2005**, *72*, 1–5. (b) Scully, S. R.; McGehee, M. D. *J. Appl. Phys.* **2006**, *100*, 1–5.

(6) Blom, P. W. M.; Mihailetchi, V. D.; Koster, L. J. A.; Markov, D. E. *Adv. Mater.* **2007**, *19*, 1551–1566.

(7) Yu, G.; Gao, J.; Hummelen, J. C.; Wudl, F.; Heeger, A. J. *Science* **1995**, *270*, 1789–1791.

(8) Jaczewska, J.; Budkowski, A.; Bernasik, A.; Moons, E.; Rysz, J. *Macromolecules* **2008**, *41*, 4802–4810.

(9) (a) Lee, J. K.; Ma, W. L.; Brabec, C. J.; Yuen, J.; Moon, J. S.; Kim, J. Y.; Lee, K.; Bazan, G. C.; Heeger, A. J. *J. Am. Chem. Soc.* **2008**, *130*, 3619–3623. (b) Peet, J.; Kim, J. Y.; Coates, N. E.; Ma, W. L.; Moses, D.; Heeger, A. J.; Bazan, G. C. *Nat. Mater.* **2007**, *6*, 497–500. (c) Yao, Y.; Hou, J. H.; Xu, Z.; Li, G.; Yang, Y. *Adv. Funct. Mater.* **2008**, *18*, 1783–1789. (d) Zhang, S.; Guo, Y.; Fan, H.; Liu, Y.; Chen, H. Y.; Yang, G.; Zhan, X.; Liu, Y.; Li, Y.; Yang, Y. *J. Polym. Sci., Polym. Chem.* **2009**, *47*, 5498–5508.

(10) (a) Chiu, M. Y.; Jeng, U. S.; Su, C. H.; Liang, K. S.; Wei, K. H. *Adv. Mater.* **2008**, *20*, 2573–2578. (b) Ma, W. L.; Yang, C. Y.; Gong, X.; Lee, K.; Heeger, A. J. *Adv. Funct. Mater.* **2005**, *15*, 1617–1622.

(11) Li, G.; Shrotriya, V.; Huang, J. S.; Yao, Y.; Moriarty, T.; Emery, K.; Yang, Y. *Nat. Mater.* **2005**, *4*, 864–868.

(12) (a) Sun, S. S. *Sol. Energy Mater.* **2003**, *79*, 257–264. (b) Gunes, S.; Neugebauer, H.; Sariciftci, N. S. *Chem. Rev.* **2007**, *107*, 1324–1338.

(13) (a) Bang, J.; Jeong, U.; Ryu, D. Y.; Russell, T. P.; Hawker, C. J. *Adv. Mater.* **2009**, 21, early view.(b) Bates, F. S.; Fredrickson, G. H. *Annu. Rev. Phys. Chem.* **1990**, *41*, 525–557. (c) Bates, F. S.; Fredrickson, G. H. *Phys. Today* **1999**, *52*, 32–38.

(14) (a) Lindner, S. M.; Huttner, S.; Chiche, A.; Thelakkat, M.; Krausch, G. *Angew. Chem., Int. Ed.* **2006**, *45*, 3364–3368. (b) Lindner, S. M.; Thelakkat, M. *Macromolecules* **2004**, *37*, 8832–8835. (c) Sommer, M.; Lindner, S. M.; Thelakkat, M. *Adv. Funct. Mater.* **2007**, *17*, 1493–1500.

(15) (a) Barrau, S.; Heiser, T.; Richard, F.; Brochon, C.; Ngov, C.; van de Wetering, K.; Hadziioannou, G.; Anokhin, D. V.; Ivanov, D. A. *Macromolecules* **2008**, *41*, 2701–2710. (b) Stalmach, U.; de Boer, B.; Videlot, C.; van Hutten, P. F.; Hadziioannou, G. *J. Am. Chem. Soc.* **2000**, *122*, 5464–5472. (c) van der Veen, M. H.; de Boer, B.; Stalmach, U.; van de wetering, K. I.; Hadziioannou, G. *Macromolecules* **2004**, *37*, 3673–3684.

(16) (a) Lee, M.; Cho, B. K.; Zin, W. C. *Chem. Rev.* **2001**, *101*, 3869–3892. (b) Matsen, M. W.; Barrett, C. *J. Chem. Phys.* **1998**, *109*, 4108–4118.

(17) (a) Olsen, B. D.; Jang, S. Y.; Luning, J. M.; Segalman, R. A. *Macromolecules* **2006**, *39*, 4469–4479. (b) Olsen, B. D.; Segalman, R. A. *Macromolecules* **2005**, *38*, 10127–10137. (c) Olsen, B. D.; Segalman, R. A. *Mater. Sci. Eng., R* **2008**, *62*, 37–66. (d) Olsen, B. D.; Shah, M.; Ganesan, V.; Segalman, R. A. *Macromolecules* **2008**, *41*, 6809–6817.

(18) Babel, A.; Jenekhe, S. A. *Macromolecules* **2004**, *37*, 9835–9840.

(19) Liu, J. S.; Sheina, E.; Kowalewski, T.; McCullough, R. D. *Angew. Chem., Int. Ed.* **2002**, *41*, 329–332.

(20) Boudouris, B. W.; Frisbie, C. D.; Hillmyer, M. A. *Macromolecules* **2008**, *41*, 67–75.

(21) (a) Yurt, S.; Anyanwu, U. K.; Scheintaub, J. R.; Coughlin, E. B.; Venkataraman, D. *Macromolecules* **2006**, *39*, 1670–1672. (b) Zhang, M. F.; Yang, L.; Yurt, S.; Misner, M. J.; Chen, J. T.; Coughlin, E. B.; Venkataraman, D.; Russell, T. P. *Adv. Mater.* **2007**, *19*, 1571–1576.

(22) Iovu, M. C.; Craley, C. R.; Jeffries-El, M.; Krankowski, A. B.; Zhang, R.; Kowalewski, T.; McCullough, R. D. *Macromolecules* **2007**, *40*, 4733–4735.

(23) Chen, X. W.; Gholamkhass, B.; Han, X.; Vamvounis, G.; Holdcroft, S. *Macromol. Rapid Commun.* **2007**, *28*, 1792–1797.

(24) Murray, K. A.; Holmes, A. B.; Moratti, S. C.; Rumbles, G. *J. Mater. Chem.* **1999**, *9*, 2109–2115.

(25) (a) Benoit, D.; Hawker, C. J.; Huang, E. E.; Lin, Z.; Russell, T. P. *Macromolecules* **2000**, *33*, 1505–1507. (b) Rodlert, M.; Harth, E.; Rees, I.; Hawker, C. J. *J. Polym. Sci., Polym. Chem.* **2000**, *38*, 4749–4763. (c) Hawker, C. J.; Barclay, G. G.; Dao, J. *J. Am. Chem. Soc.* **1996**, *118*, 11467–11468. (d) Dao, J.; Benoit, D.; Hawker, C. J. *J. Polym. Sci., Polym. Chem.* **1998**, *36*, 2161–2167.

(26) (a) Banishoeib, F.; Henckens, A.; Fourier, S.; Vanhooyland, G.; Breselge, M.; Manca, J.; Cleij, T. J.; Lutsen, L.; Vanderzande, D.; Nguyen, L. H.; Neugebauer, H.; Sariciftci, N. S. *Thin Solid Films* **2008**, *516*, 3978–3988. (b) Krasovskiy, A.; Knochel, P. *Angew. Chem., Int. Ed.* **2004**, *43*, 3333–3336.

(27) Loewe, R. S.; Khersonsky, S. M.; McCullough, R. D. *Adv. Mater.* **1999**, *11*, 250–253.

(28) (a) Costanzo, P. J.; Stokes, K. K. *Macromolecules* **2002**, *35*, 6804–6810. (b) Kim, K. H.; Jo, W. H. *Macromolecules* **2007**, *40*, 3708–3713.

(29) Liu, J. S.; Loewe, R. S.; McCullough, R. D. *Macromolecules* **1999**, *32*, 5777–5785.

(30) Patil, A. O.; Heeger, A. J.; Wudl, F. *Chem. Rev.* **1988**, *88*, 183–200.

(31) Bartus, J. *J. Macromol. Sci., Part A: Pure Appl. Chem.* **1991**, *A28*, 917–924.

(32) Ziemelis, K. E.; Hussain, A. T.; Bradley, D. D. C.; Friend, R. H.; Ruhe, J.; Wegner, G. *Phys. Rev. Lett.* **1991**, *66*, 2231–2234.

(33) (a) Beaucage, G. *J. Appl. Crystallogr.* **1995**, *28*, 717–728. (b) Beaucage, G. *J. Appl. Crystallogr.* **1996**, *29*, 134–146.

(34) (a) van Duren, J. K. J.; Yang, X. N.; Loos, J.; Bulle-Lieuwma, C. W. T.; Sieval, A. B.; Hummelen, J. C.; Janssen, R. A. J. *Adv. Funct. Mater.* **2004**, *14*, 425–434. (b) Yokoyama, H.; Kramer, E. J.; Rafailovich, M. H.; Sokolov, J.; Schwarz, S. A. *Macromolecules* **1998**, *31*, 8826–8830.